Nitrogenases

International Edition: DOI: 10.1002/anie.201600010
German Edition: DOI: 10.1002/ange.201600010

Nitrogenases—A Tale of Carbon Atom(s)

Yilin Hu and Markus W. Ribbe**

Keywords:
C–C coupling · CO activation · interstitial carbide · nitrogenases · radicals

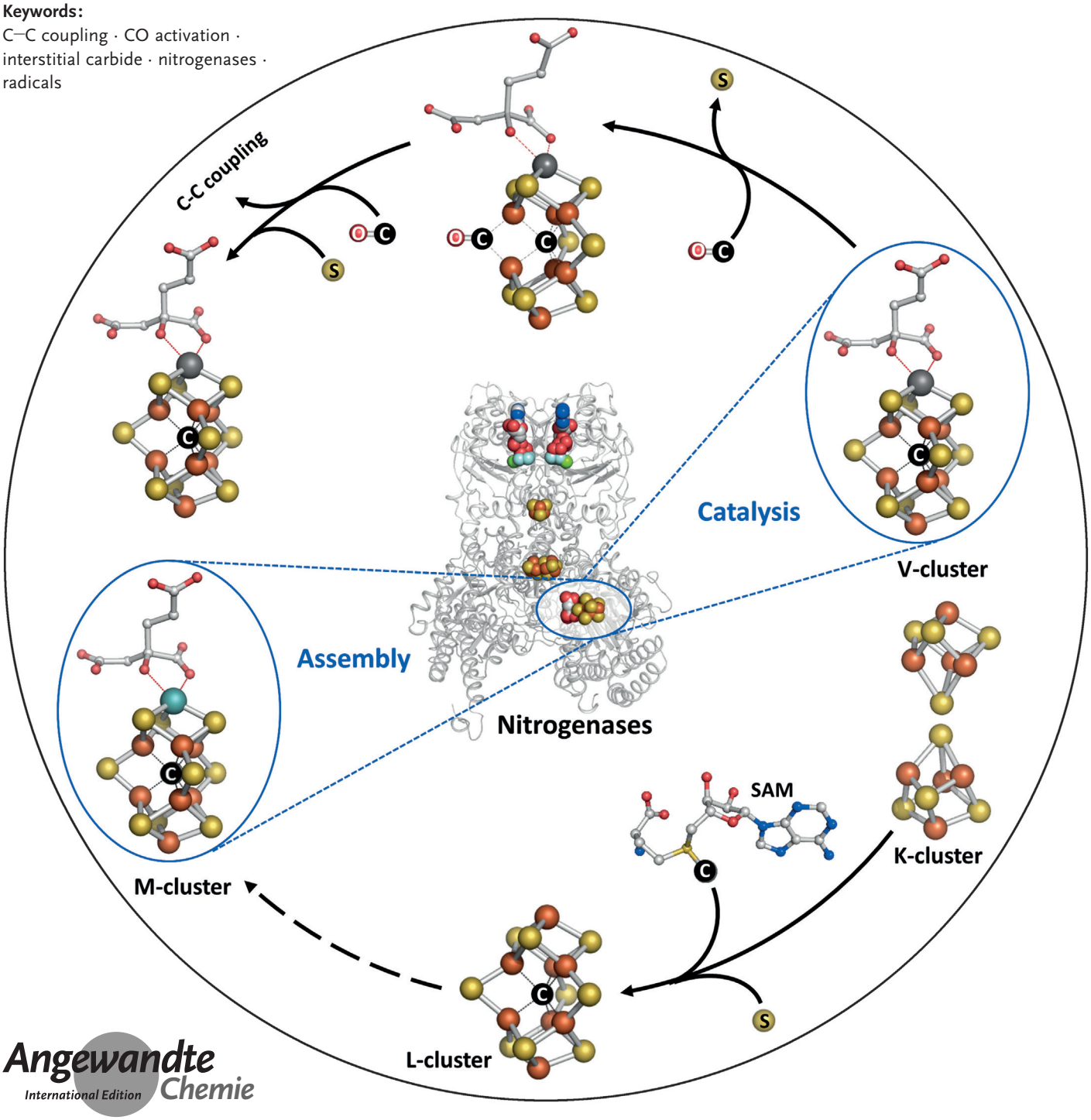

© 2016 Wiley-VCH Verlag GmbH & Co. KGaA, Weinheim

Named after its ability to catalyze the reduction of nitrogen to ammonia, nitrogenase has a surprising rapport with carbon—both through the interstitial carbide that resides in the central cavity of its cofactor and through its ability to catalyze the reductive carbon–carbon coupling of small carbon compounds into hydrocarbon products. Recently, a radical-SAM-dependent pathway was revealed for the insertion of carbide, which signifies a novel biosynthetic route to complex bridged metalloclusters. Moreover, a sulfur-displacement mechanism was proposed for the activation of carbon monoxide by nitrogenase, which suggests an essential role of the interstitial carbide in maintaining the stability while permitting a certain flexibility of the cofactor structure during substrate turnover.

From the Contents

1. Introduction

Nitrogenase is a complex metalloenzyme that plays a key role in the global nitrogen cycle, catalyzing the reduction of the inert nitrogen (N_2) to the bio-accessible ammonia (NH_3) in a reaction usually depicted by Equation (1) (ADP = adenosine diphosphate, ATP = adenosine triphosphate. P_i = inorganic phosphate.[1–3] Recently, it was demonstrated that nitrogenase was also capable of reducing small carbon-containing molecules, such as carbon monoxide (CO) and carbon dioxide (CO_2),[4] to hydrocarbons, thereby defining nitrogenase as a versatile reductase of both nitrogen- and carbon-containing compounds.[5–8] The reductions of nitrogen and carbon compounds by nitrogenase resemble each other in that they both use proton (H^+)/electron (e^-) pairs as the reducing power and they both occur at ambient temperature and pressure. The two types of nitrogenase-enabled reactions have their respective equivalents in the industrial Haber–Bosch and Fischer–Tropsch processes. In contrarst to the nitrogenase-based reactions, both industrial processes occur at high temperatures and pressures: the former combines N_2 and hydrogen (H_2) into ammonia,[9] whereas the latter combines CO (a typical substrate)/CO_2 (an atypical substrate) and H_2 into hydrocarbon-based carbon fuels.[10] The fact that nitrogenase can activate N_2, CO, and CO_2 under ambient conditions suggests the potential of this enzyme as an attractive template for the future design of cost-efficient strategies to convert these small molecules into products of agronomic and economic values.

$$N_2 + 8\,H^+ + 8\,e- + 16\,MgATP \rightarrow 2\,NH_3 + H_2 + 16\,MgADP + 16\,P_i \quad (1)$$

Perhaps equally as interesting, the reactivity of nitrogenase toward nitrogen and carbon compounds points to a plausible role of this enzyme as an evolutionary link between the nitrogen and carbon cycles on Earth. It is possible that nitrogenase functioned as a CO_2/CO reductase in a CO_2-rich atmosphere early on and evolved later into an N_2 reductase while retaining certain activity as a CO_2/CO reductase as photosynthesis emerged.

The reactivity of nitrogenase toward carbon compounds has drawn considerable attention since its discovery, as it bears significant relevance to the development of the much-sought-after approaches to recycle carbon waste (CO) and greenhouse gas (CO_2) into useful chemical and fuel products. The fundamental importance of this reactivity have prompted questions as to whether there is an intrinsic correlation between nitrogenase and carbon species and, if so, how it is related to the ability of nitrogenase to handle carbon-containing molecules. Along this line of inquiry, a carbide ion has been identified as a structural element of the cofactor (designated the M-cluster) of Mo-nitrogenase. Often referred to as the "conventional" member of the nitrogenase family, the Mo-nitrogenase of *Azotobacter vinelandii* consists of a reductase component and a catalytic component.[1] The reductase component, designated the Fe protein (NifH), is a γ_2-dimer containing a subunit-bridging $[Fe_4S_4]$ cluster and an MgATP-binding site within each subunit; the catalytic component, designated the MoFe protein (NifDK), is an $\alpha_2\beta_2$-tetramer containing two complex metalloclusters per $\alpha\beta$-dimer: a P-cluster ($[Fe_8S_7]$) at the α/β-subunit interface and an M-cluster ($[MoFe_7S_9C$-homocitrate$]$) within the α-subunit.[11–14] Catalysis by the Mo-nitrogenase involves the formation of a functional complex between NifH and NifDK[15,16] as well as the ATP-dependent, interprotein transfer of electrons from the $[Fe_4S_4]$ cluster of NifH, via the P-cluster, to the M-cluster of NifDK, where substrate reduction occurs upon accumulation of a sufficient number of electrons (Figure 1a).

Arguably the most complex metallocofactor utilized by any known biological system, the M-cluster is ligated by only two ligands, $Cys^{\alpha 275}$ and $His^{\alpha 442}$, within the α-subunit of

[*] Prof. Dr. Y. Hu, Prof. Dr. M. W. Ribbe
Department of Molecular Biology and Biochemistry
Department of Chemistry, University of California, Irvine
Irvine, CA 92697-3900 (USA)
E-mail: yilinh@uci.edu
mribbe@uci.edu

 © 2016 Wiley-VCH Verlag GmbH & Co. KGaA, Weinheim

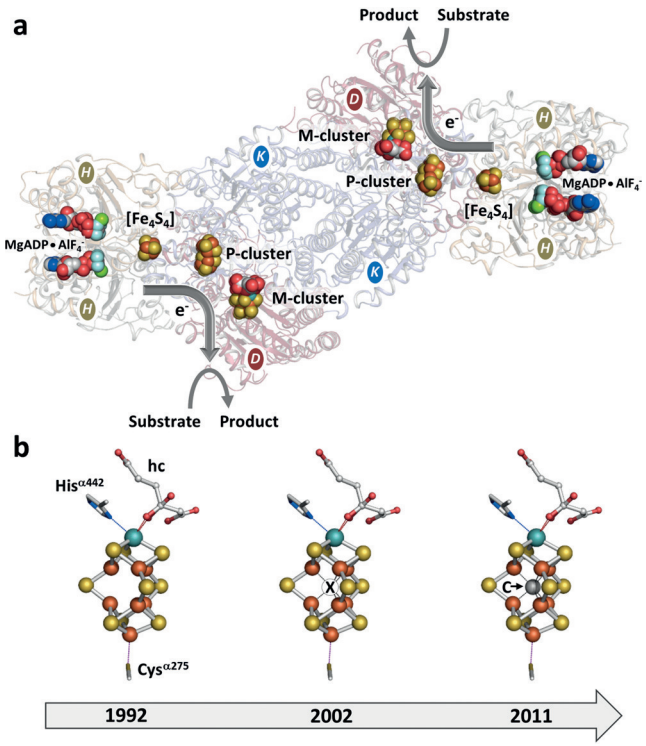

Figure 1. Structure of Mo-nitrogenase and its associated metal centers. a) Ribbon presentation (transparent) of the MgADP·AlF_4^--stabilized NifH/NifDK complex. Key components involved in electron transfer, including MgADP·AlF_4^-, $[Fe_4S_4]$ cluster, P-cluster, and M-cluster, are shown as space-filling models. The two subunits of NifH are labeled as H and colored gray and gold; the α- and β-subunits of the NifDK are labeled as D and K, respectively, and colored red and light blue. b) Structure of the M-cluster based on the crystallographic data from 1992, 2002, and 2011. $His^{\alpha 442}$ and $Cys^{\alpha 275}$, the two protein ligands of the M-cluster, are indicated. Atoms of all clusters are colored as follows: Fe orange, S yellow, Mo cyan, O red, C gray, N blue, Mg green, Al beige, F light blue. hc = homocitrate. PYMOL was used to create this figure (PDB IDs: 1N2C, 1M1N, 3U7Q).

NifDK. The M-cluster comprises a $[MoFe_7S_9]$ core that can be viewed as $[Fe_4S_3]$ and $[MoFe_3S_3]$ subcubanes bridged by three μ_2-sulfides in between. In addition, the M-cluster is further coordinated by the 2-hydroxy and 2-carboxy groups of an organic homocitrate moiety at the Mo end (Figure 1b).[11–13] The central cavity of the M-cluster had long been considered a big "void"[13] until 2002, when a high-resolution crystal structure of NifDK (1.16 Å) revealed the presence of some electron density in this void that could originate from N, O, or C.[11] This interstitial atom—designated X at the time of discovery to reflect its unknown identity—was identified later through combined spectroscopic and structural analyses as a μ_6-coordinated carbide (C^{4-}) ion (Figure 1b).[12,14] The presence of an interstitial carbide at the heart of the M-cluster further highlights the structural complexity of this metallocofactor that underlies the functional versatility of nitrogenase. Furthermore, the strategic location and unexpected identity of this interstitial atom generated excitement and interest in elucidating the relevance of this atom to the biosynthetic and catalytic mechanisms of nitrogenase, thus raising questions of where this carbide originates from, how it is incorporated into the M-cluster, and if it has any bearing on the reactivity toward carbon compounds.

2. Nitrogenase and Carbon: The Interstitial Carbide of the Nitrogenase Cofactor

Ever since its discovery, the origin of the interstitial carbide, as well as the mechanism of carbide insertion, has remained a topic of substantial interest for the specific area of nitrogenase and the general field of bioinorganic chemistry. Most knowledge about this interstitial atom was derived from studies on the biosynthesis of the M-cluster,[17–20] the active cofactor center of the Mo-nitrogenase.

2.1. Biosynthesis of the M-Cluster

The biosynthesis of the M-cluster is a complicated process that involves participation of a number of *nif*-encoded (Nif) proteins.[20] Biochemical and genetic analyses narrowed the key players in this process down to a minimum set of Nif proteins, which in turn led to the proposal of a core biosynthetic pathway of the M-cluster (Figure 2).[20] This process is initiated by NifS and NifU, which have complementary functions in mobilizing Fe and S for the formation of small FeS fragments. NifS is believed to function in the capacity of a pyridoxal-dependent cysteine desulfurase, forming a protein-bound cysteine persulfide that is subsequently donated to NifU for the sequential formation of

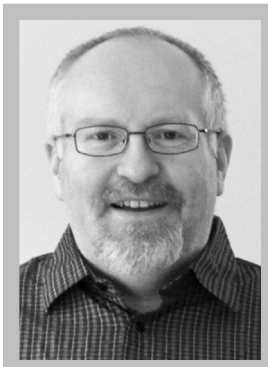

Markus W. Ribbe received a BS in Biology, a MS in Microbiology, and a PhD in Microbiology from the University of Bayreuth, Germany, with Prof. O. Meyer. He was a postdoctoral fellow in the group of Prof. B. K. Burgess at the University of California, Irvine, where he is now Chancellor's Professor. During the past 20 years, he has focused on the mechanistic investigation of nitrogenase catalysis and assembly using combined biochemical, spectroscopic, and structural approaches. The current Review is based on the lecture he gave at the 50th Anniversary of the Bürgenstock Conference 2015.

Yilin Hu received a BS in Genetics from Fudan University, China, and a PhD in Biochemistry with Prof. C. W. Slattery from Loma Linda University (USA). She was a postdoctoral fellow in the group of Prof. Barbara K. Burgess at the University of California, Irvine, where she is currently Assistant Professor. During the last 12 years, she has focused on studies related to nitrogenase mechanism and assembly, with an emphasis on the genetic manipulation of nitrogenase systems.

© 2016 Wiley-VCH Verlag GmbH & Co. KGaA, Weinheim

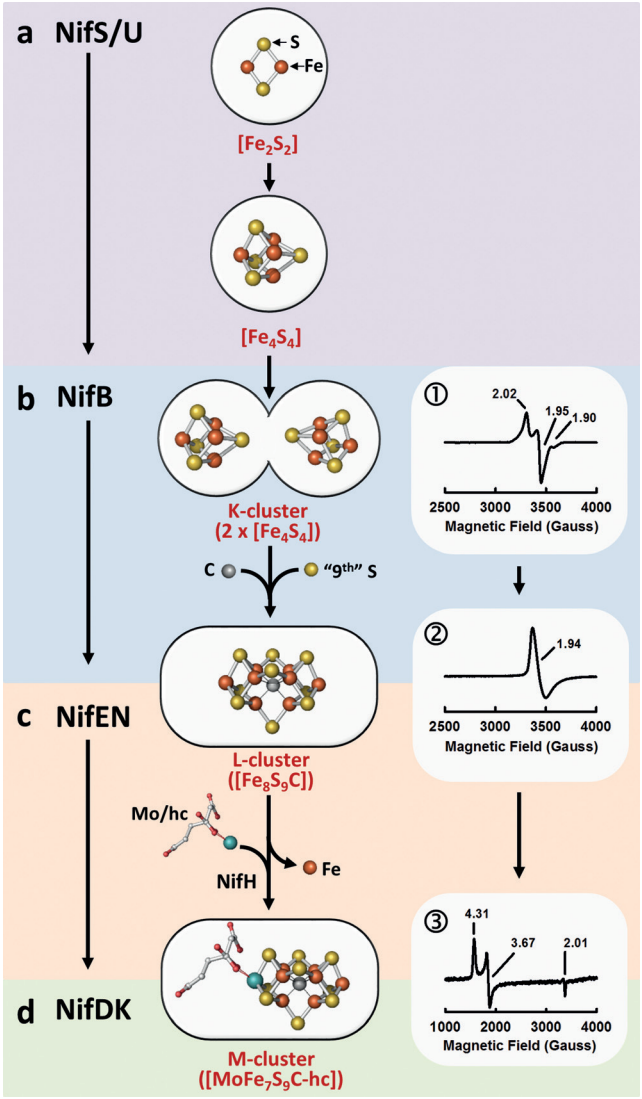

Figure 2. Biosynthesis of the M-cluster of Mo-nitrogenase. Actions of a number of assembly-related Nif proteins lead to a) formation of $[Fe_2S_2]$ and $[Fe_4S_4]$ clusters on NifS/U; b) generation of the L-cluster ($[Fe_8S_9C]$) on NifB; c) insertion of Mo and homocitrate (hc) by NifH into the L-cluster, which give rise to a mature M-cluster ($[MoFe_7S_9C$-hc]) on NifEN; and d) delivery of the M-cluster to its target location in NifDK. NifB catalyzes the K- to L-cluster conversion, which involves radical-SAM-dependent carbide insertion concomitant with the insertion of a ninth sulfur atom and the rearrangement/coupling of the two 4Fe units of the K-cluster into an 8Fe L-cluster. The characteristic EPR features of ① K-, ② L-, and ③ M-clusters are shown next to the corresponding structural models.

$[Fe_2S_2]$ and $[Fe_4S_4]$ clusters (Figure 2a).[21–26] Following this event, a $[Fe_4S_4]$ cluster pair (designated the K-cluster) is transferred from NifU to NifB, where it is converted into a $[Fe_8S_9C]$ cluster (designated the L-cluster) that closely resembles the metal–sulfur core of the M-cluster except for the substitution of an Fe atom for the Mo-homocitrate "conjugate" at one end of the cluster (Figure 2b,c).[27–31] The L-cluster is then transferred from NifB to NifEN and matured into an M-cluster upon ATP-dependent insertion of Mo and homocitrate by NifH prior to the delivery of the fully assembled M-cluster to its target location in NifDK (Figure 2c,d).[32–35]

Such a biosynthetic pathway was pieced together with the help of strategic deletions of *nif* genes,[20,36] which facilitated capture of the biosynthetic intermediates of the M-cluster by key Nif proteins. Subsequent EPR and biochemical analyses revealed the sequential transformation of the K→L→M cluster in this process (Figure 2, ①–③), which could be monitored by a change in the EPR features from the K-cluster-specific $S=1/2$ signal ($g=2.02$, 1.95, and 1.90) to the L-cluster-specific signal ($g=1.94$) to the M-cluster-specific $S=3/2$ signal ($g=4.31$, 3.67, and 2.01), as well as an accompanying change in the metal content and reconstitution activities of these cluster species.[19,26,31,33,34] XAS/EXAFS and crystallographic studies provided further insights into the structures of the biosynthetic intermediates of the M-cluster, thus demonstrating the formation of a complete 8Fe core of the M-cluster (i.e. the L-cluster) prior to the substitution of Mo and homocitrate for one terminal Fe atom of the 8Fe core (Figure 2c,d).[28–31] Furthermore, these studies established NifH—better known as the reductase component of Mo-nitrogenase—as an ATP-dependent Mo/homocitrate insertase capable of transforming the L-cluster into a fully matured M-cluster (Figure 2).[33] Together, these observations have defined the strategy of M-cluster biosynthesis as a variation on the theme of the stepwise fusion of FeS modules, during which process 2Fe, 4Fe, and 8Fe platforms are generated in sequence along with the incorporation of C and S (Figure 2b,c) and the substitution of one Fe atom of the 8Fe core by Mo/homocitrate (Figure 2c,d). The insertion of carbide is of particular interest, as it plays a pivotal role in a complex synthetic strategy that is used to generate the complete core structure of the M-cluster.

2.2. Incorporation of the Interstitial Carbide

The incorporation of the interstitial carbide into the M-cluster is catalyzed by NifB, an indispensable player in the process of cofactor assembly. The first indication of the essential role of NifB in this process came from the observation that deletion of the *nifB* gene resulted in the formation of an M-cluster-deficient form of NifDK (designated apo-NifDK).[37,38] Subsequent sequence analyses of NifB revealed the presence of a CxxxCxxC motif for the coordination of an *S*-adenosylmethionine (SAM) binding $[Fe_4S_4]$ cluster (designated the SAM cluster), as well as a sufficient amount of additional ligands for the accommodation of the two $[Fe_4S_4]$ modules of the K-cluster, thus leading to the hypothesis that NifB employs radical-SAM chemistry to couple the two 4Fe units of the K-cluster into an 8Fe L-cluster.[20,39] Consistent with this hypothesis, EPR analysis demonstrated that the K-cluster-specific, $S=1/2$ signal disappeared concomitant with the appearance of the L-cluster-specific $g=1.94$ signal (Figure 2) upon incubation of NifB with SAM,[27] thereby providing the initial evidence for the SAM-dependent nature of the transformation from a K-cluster (2×4Fe) into an L-cluster (8Fe).

 © 2016 Wiley-VCH Verlag GmbH & Co. KGaA, Weinheim

The role of SAM in this process was further examined by HPLC analysis of the products of SAM cleavage by NifB. Two products were detected following the incubation of SAM with NifB: one, *S*-adenosylhomocysteine (SAH), was formed upon removal of the methyl group of SAM; the other, 5′-deoxyadenosine (5′-dAH), was generated upon abstraction of a hydrogen atom by a 5′-deoxyadenosyl radical (5′-dA•; Figure 3, ①).[19,20] This observation suggests the participation of two SAM molecules in the NifB-catalyzed K→L cluster conversion: one of them serves as the donor of a methyl group that eventually gives rise to the interstitial carbide, whereas the other is used to generate a 5′-dA• radical that abstracts a hydrogen atom from the methyl group to initiate the radical-dependent process of carbide insertion.

Isotope labeling experiments supplied proof for this argument, demonstrating the incorporation of the ^{14}C label of [^{14}C]methyl-SAM into the L-cluster concomitant with the conversion of the K- to L-cluster on NifB,[19,20] as well as the formation of deuterated 5′-deoxyadenosine (5′-dAD) when [D_3]methyl-SAM was used as a methyl donor in this process (Figure 3, ②).[19,20] In combination, these results firmly establish that the source of the interstitial carbide is the methyl group of SAM (Figure 3a), which undergoes an initial hydrogen atom abstraction by a 5′-dA• radical (Figure 3b) before the ensuing carbon intermediate is eventually processed into an interstitial carbide upon further deprotonation/dehydrogenation (Figure 3c).[20]

The early events of carbide insertion were further explored to determine the location of the methyl attachment and the sequence of events between methyl transfer and hydrogen abstraction. Interestingly, methanethiol (CH_3SH) and [D_3]methanethiol (CD_3SH) were detected as the respective products of acid quenching following the incubation of NifB with unlabeled SAM (Figure 3, ③) and [D_3]methyl-SAM (Figure 3, ④, thus suggesting the attachment of a SAM-derived methyl group to an acid-labile sulfur atom of the NifB-associated K-cluster.[17] Moreover, substitution of the sulfur atoms of the K-cluster by selenium (Se) led to the formation of methylselenol (CH_3SeH)—the Se-substituted form of methylthiol—in the same reaction, thus providing additional support for the transfer of a methyl group to a sulfur atom of the K-cluster (Figure 3, ⑤).[17] Incubation of NifB with allyl-SAM, a SAM analogue containing an allyl group (-CH-CH=CH_2) in place of the methyl group (-CH_3), generated SAH as the sole product of SAM cleavage. However, the absence of hydrogen abstraction from the allyl group by a 5′-dA• radical did not prevent the formation of allylthiol (CH_2=CH-CH-SH)—the allyl-substituted form of methylthiol—upon acid quenching (Figure 3, ⑥).[17] This observation suggests that transfer of the allyl group from allyl-SAM occurs independently from the event of hydrogen atom abstraction. Thus, by analogy, transfer of the methyl group from SAM follows an S_N2-type mechanism, whereby the complete methyl group is transferred to the sulfur atom of the K-cluster before it is processed into a carbon intermediate—likely a methylene radical—upon abstraction of a hydrogen atom by a 5′-dA• radical (Figure 3a,b).

Although steps of the carbide insertion pathway prior to the hydrogen abstraction have been refined through these studies, the subsequent events along this pathway remain elusive. It is not clear how the methyl-derived carbon intermediate is further processed into a carbide ion. In addition, the origin of the ninth sulfur atom and how it is incorporated as a cluster-bridging sulfide to complete the stoichiometry of the L-cluster are not understood. Perhaps the most important question, however, is how radical

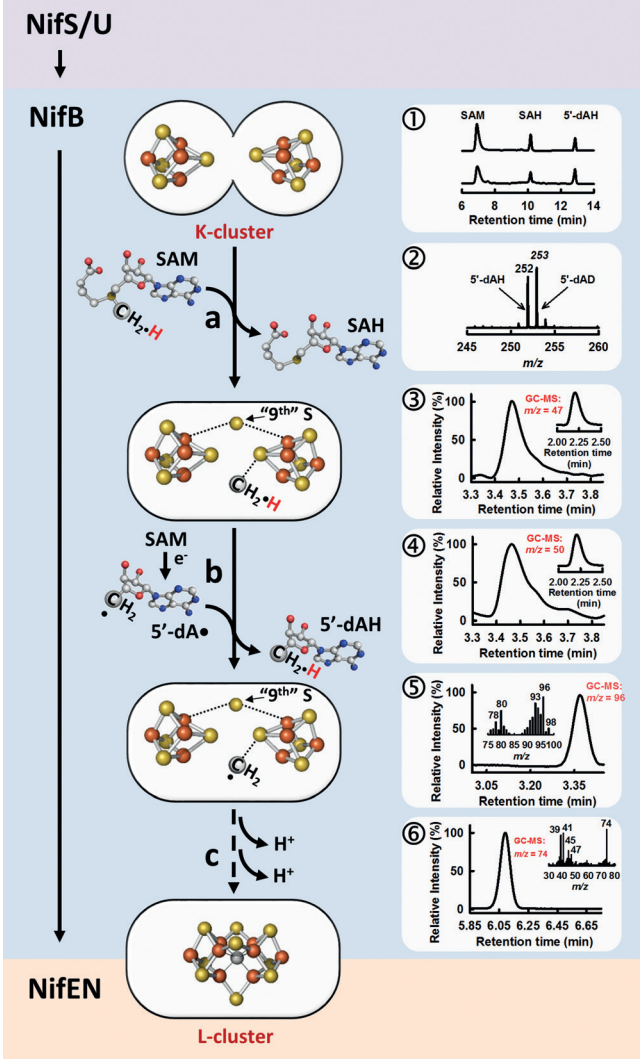

Figure 3. Formation of the L-cluster on NifB. Carbide insertion presumably begins with methyl transfer from one SAM molecule to a sulfide atom of the K-cluster (a), followed by hydrogen abstraction from this methyl group by a 5′-dA• radical that is derived from homolytic cleavage of a second SAM molecule (b). The resulting, cluster-bound carbon intermediate (e.g. a methyl radical) then initiates radical-based chemical rearrangement/coupling of the two [Fe_4S_4] modules of the K-cluster into a [Fe_8S_9C] L-cluster concomitant with the insertion of a ninth sulfur atom and further dehydrogenation/deprotonation of the carbon intermediate until a carbide ion appears in the center of the L-cluster (c). ① HPLC profile of the standards (top) and the actual products of SAM cleavage by NifB (bottom); ② LC-MS analysis of the 5′-dA species generated upon incubation of NifB with [D_3]methyl-SAM; ③–⑥ GC-MS analyses of products generated upon acid quenching of reactions containing ③ NifB and SAM; ④ NifB and [D_3]methyl-SAM; ⑤ Fe/Se-reconstituted NifB and SAM; and ⑥ NifB and allyl-SAM.

 © 2016 Wiley-VCH Verlag GmbH & Co. KGaA, Weinheim

chemistry—initiated by the formation of a cluster-bound, radical carbon intermediate upon abstraction of a hydrogen atom—enables the coupling and restructuring of the two 4Fe modules of the K-cluster into an 8Fe L-cluster concomitant with the insertion of both the interstitial carbide and the ninth sulfur atom. Although facile ligand replacement of the tetrahedral Fe^{2+}/Fe^{3+} atoms through an addition/elimination mechanism can be hypothesized for the required structural rearrangement for the formation of an L-cluster,[40,41] the exact details of this radical-based process are yet to be explored. Regardless, the unique chemistry utilized in this process not only establishes NifB as a new member of the radical SAM methyltransferase family that specializes in the assembly of metallocofactors,[39] but also places carbide insertion at the strategic point of a previously unobserved, radical-SAM-dependent biosynthetic route to complex, bridged metalloclusters.

3. Nitrogenase and Carbon: Reductive C–C Coupling by Nitrogenase

The relationship between nitrogenase and carbon goes well beyond the presence of a central carbide at the heart of the active cofactor site of this metalloenzyme. Studies in recent years have established nitrogenase as a "reductive C–C couplase" that is capable of reducing small carbon compounds (CO and CO_2) to hydrocarbons [alkenes (C_nH_{2n}) and alkanes (C_nH_{2n+2})] under ambient conditions,[5–8,42–46] which generated substantial interest in exploring the relevance of this enzyme to environment improvement and energy production. Interestingly, although the N_2-reducing activity was initially established for the "conventional" Mo-nitrogenase, the CO-reducing activity was first discovered in the "alternative" V- nitrogenase from *A. vinelandii*.[7] The V-nitrogenase is a natural variant of the Mo-nitrogenase, and the two nitrogenases share a good degree of homology with regard to the primary sequences of their subunits and the structural compositions of their metallocenters.[47,48] Similar to its Mo counterpart (Figure 4a), the V-nitrogenase consists of a reductase component [designated the Fe protein (VnfH)] and a catalytic component [designated the VFe protein (VnfDGK); Figure 4c]. Substrate turnover by V-nitrogenase (Figure 4c), similar to that by Mo-nitrogenase (Figure 4a), involves the formation of a functional complex between the two protein components[1–3,47,48] and the subsequent ATP-dependent, interprotein transfer of electrons from the reductase component to the cofactor site of the catalytic component, where substrate reduction takes place.

The Mo- and V-nitrogenases have a set of homologous clusters.[48] The respective reductase components of the two nitrogenases (i.e. NifH and VnfH) contain nearly indistinguishable $[Fe_4S_4]$ clusters (Figure 4b,c, top);[16,48,49] similarly, the respective catalytic components of these nitrogenases (i.e. NifDK and VnfDGK) contain homologous P-cluster species (i.e. P- and P^V-clusters) and cofactor centers (i.e. M- and V-clusters). The P- and P^V-clusters are 8Fe clusters of similar topology (Figure 4b,d, middle);[5,16,48,50] whereas the M- and V-clusters not only resemble each other in terms of cluster composition and core structure (Figure 4b,d, bottom),[12–14,47,48,51] but also contain the same interstitial carbide ion (Figure 4e)[52] that further accentuates the

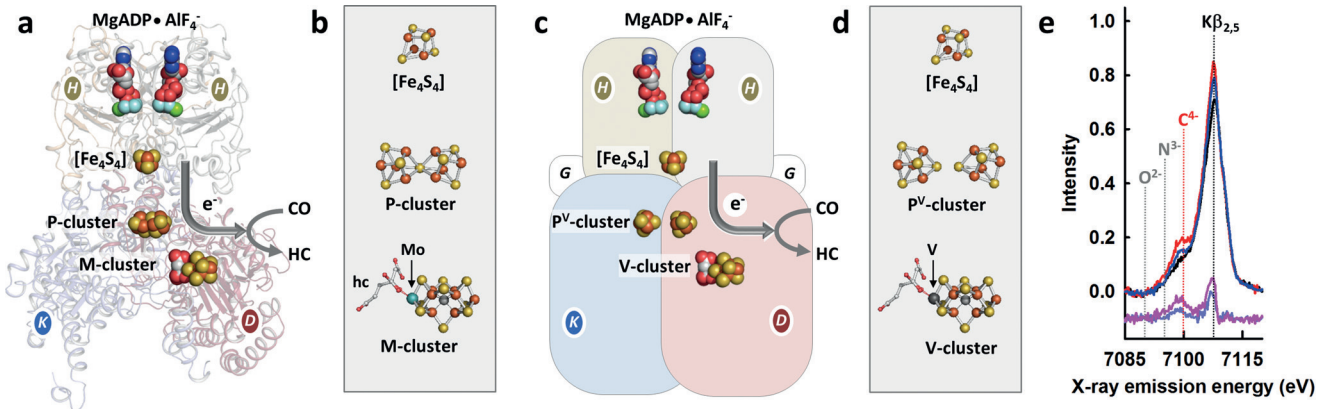

Figure 4. Comparison of the structures of Mo- and V-nitrogenases and their associated metal centers. a) Ribbon presentation (transparent) of the $^1/_2$ $MgADP{\cdot}AlF_4^-$-stabilized NifH/NifDK complex. Key components involved in electron transfer, including $MgADP{\cdot}AlF_4^-$, $[Fe_4S_4]$ cluster, P-cluster, and M-cluster, are shown as space-filling models. b) The structures of the $[Fe_4S_4]$ cluster, P-cluster, and M-cluster shown as ball-and-stick models. c) Schematic presentation of the $^1/_2$ $MgADP{\cdot}AlF_4^-$-stabilized VnfH/VnfDGK complex. Key components involved in electron transfer, including $MgADP{\cdot}AlF_4^-$, $[Fe_4S_4]$ cluster, P^V-cluster, and V-cluster, are shown as space-filling models. d) The structures of $[Fe_4S_4]$ cluster, P^V-cluster, and V-cluster shown as ball-and-stick models. The structure of Mo-nitrogenase was rendered based on X-ray crystallographic data (PDB ID: 1N2C); whereas the hypothetical structure of V-nitrogenase was rendered based on available biochemical and spectroscopic data. The subunits and atoms of both nitrogenases are colored as described in Figure 1. Additionally, the δ-subunit of VnfDGK is labeled as G and shown in white, and V is colored dark gray. The structures of the clusters shown in (a) and (b) are based on crystallographic data,[11–13,15,16] while the structures of the clusters shown in (c) and (d) are based on XAS/EXAFS data.[48–51] PYMOL was used to create the structural models in this figure (PDB IDs: 1N2C, 1M1N, 3U7Q). HC: hydrocarbons. e) K-valence XES spectra of the V-cluster (red), holo VnfDGK (blue), and apo VnfDGK (black), as well as difference spectra (offset for clarity) of V-cluster/apo-VnfDGK (magenta) and holo-/apo-VnfDGK (gray/blue). The dashed lines denote the calculated energy positions for M-clusters containing interstitial C^{4-}, N^{3-}, and O^{2-}, respectively, relative to the $K\beta_{2,5}$ line.[52] The role of Mo or V in nitrogenase catalysis is unclear, although it has been proposed that the heterometal could function in modulating the redox properties of the cofactor.

 © 2016 Wiley-VCH Verlag GmbH & Co. KGaA, Weinheim

structural homology between the two cofactors. There are, however, clear differences between the two homologous nitrogenases, particularly with regard to the cluster species that reside in their respective catalytic components. Compared to the [Fe_8S_7] structure of the P-cluster of the Mo-nitrogenase (Figure 4b middle), the P^V-cluster of the V-nitrogenase consists of a [Fe_4S_4]-like cluster pair (Figure 4d, middle) that assumes a more open conformation at the α/β-interface of VnfDGK (see Figure 4c). Likewise, despite a close resemblance to the M-cluster in the Mo-nitrogenase (Figure 4b, bottom), the V-cluster of the V-nitrogenase contains V in place of Mo and has a somewhat altered electronic structure (Figure 4d, bottom).[51] The similarities and dissimilarities between the two nitrogenases render them similar yet distinct in their catalytic abilities; most notably, the V-nitrogenase is substantially more active than its Mo counterpart in catalyzing the conversion of CO into hydrocarbons, despite being less active than the latter in catalyzing the reduction of N_2 to NH_3.

3.1. ATP-Dependent Reduction of CO and CO_2

Working as a two-component enzyme system, the V-nitrogenase is capable of catalyzing the ATP-dependent reduction of CO to methane (CH_4), ethene (C_2H_4), ethane (C_2H_6), propene (C_3H_6), propane (C_3H_8), butene (C_4H_8), and butane (C_4H_{10}) in the presence of both H_2O and D_2O (Figure 5a).[6,7] The turnover numbers (TONs) of the V-nitrogenase-catalyzed reduction of CO are 992 h^{-1} and 1108 h^{-1} in H_2O and D_2O, respectively, with C_2 hydrocarbons being the predominant products in both cases (Figure 5c).[6] In comparison, the Mo-nitrogenase can only reduce CO to CH_4, C_2H_4, C_2H_6, C_3H_6, and C_3H_8 (Figure 5a) at a TON of 1 h^{-1} (Figure 5c) in the presence of H_2O.[6] Substitution of D_2O for H_2O adds C_4H_8 and C_4H_{10} to the product profile of the Mo-nitrogenase-catalyzed reduction of CO (Figure 5a), and the expansion of the product profile is accompanied by a significant increase in the TON of this reaction to 27 h^{-1} (Figure 5c).[6] However, despite following a similar pattern of product distribution, the Mo-nitrogenase is considerably less active than the V-nitrogenase in the ATP-dependent conversion of CO into hydrocarbons, with activities of 0.1% and 2% of those of its V-counterpart in H_2O and D_2O, respectively (Figure 5c).

Compared to CO, CO_2 is an extremely poor substrate for both V- and Mo-nitrogenases. The two nitrogenases facilitate the ATP-dependent reduction of CO_2 to CO and hydrocarbons[43] at comparable efficiencies in H_2O and D_2O, with the widest product profile (CO, CH_4, C_2H_4, and C_2H_6) and the highest TON (0.25 h^{-1}) achieved by the V-nitrogenase in D_2O (Figure 5b,d).[43] Moreover, the reduction of CO_2 by both nitrogenases generate mostly C_1 products (CO and CH_4), and substitution of H_2O by D_2O pushes the reactions of both nitrogenases toward an increased formation of CO (Figure 5b,d).[43] It is interesting to note that at least part of the CH_4 generated in the nitrogenase-based reduction does not originate from CO_2, thereby leading to the speculation that the interstitial carbide may serve as the carbon source of some of the CH_4 that is generated in this reaction.[43] If this were the case, it could be argued that removal of the central carbide—possibly upon a change of the pH value that results from CO_2 dissolved in aqueous solutions—contributes to an increased instability of the cluster, which in turn accounts for the poor reactivity of nitrogenase toward CO_2 in H_2O. This argument would also be consistent with a significant increase in the CO_2 reduction by isolated nitrogenase cofactors in an organic solvent (see Section 3.2).

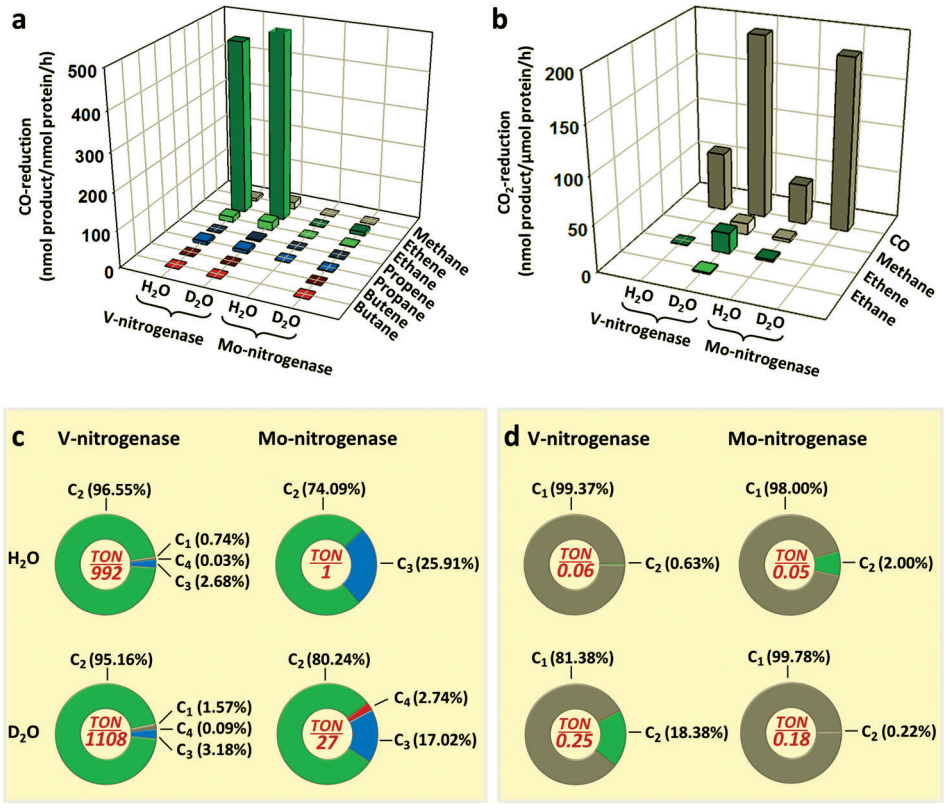

Figure 5. ATP-dependent reduction of CO and CO_2 by V- and Mo-nitrogenases. Shown are the activities of product formation (a, b) and the profiles of products (c, d) of the reactions of CO (a, c) and CO_2 (b, d) reduction by nitrogenases in the presence of H_2O and D_2O. The product profiles (c, d) show the percentages of C_1, C_2, C_3, and C_4 products. The TON was calculated from the nmol of reduced carbon that appeared in the hydrocarbon products per nmol NifDK (Mo-nitrogenase) or VnfDGK (V-nitrogenase).

© 2016 Wiley-VCH Verlag GmbH & Co. KGaA, Weinheim

3.2. ATP-Independent Reduction of CO and CO_2

The ability of nitrogenase to reduce CO and CO_2 has prompted investigation into the possibility of utilizing the cofactor of nitrogenase as a stand-alone catalyst for the ambient conversion of CO and CO_2 into hydrocarbons. By using a previously established method,[53] both M- and V-clusters have been extracted as intact entities into an organic solvent, *N*-methylformamide (NMF).[51] In addition, the L-cluster (Figure 2)—which is both a biosynthetic precursor and an all-iron structural homologue of the mature cofactor—was also successfully isolated in NMF,[29] thus adding another interesting cofactor-related species that could be examined for substrate-reducing activities. Importantly, all three cofactor species remained relatively stable in the isolated state, likely because of the presence of an interstitial carbide—its μ_6-coordination to six Fe atoms of the cofactor loosely resembling that of carbide coordination in steel—in the central cavities of all three clusters.

The structural integrity of the isolated cofactor species provides a strong basis for their functionalities as catalysts for the ATP-independent reduction of CO and CO_2. All three clusters are capable of reducing CO to hydrocarbons in aqueous buffer systems in the presence of europium(II) diethylenetriaminepentaacetic acid (Eu^{II}-DTPA; $E^{0\prime} = -1.14$ at pH 8.0); however, all three reactions occur at subcatalytic levels (i.e. TON < 1; Figure 6a).[44,46] When samarium(II) iodide [SmI_2; $E^{0\prime} = -1.55$ in tetrahydrofuran (THF)] and 2,6-lutidinium triflate (Lut-H) are used as the respective reductant and proton sources, all three clusters can reduce CO to CH_4, C_2H_4, C_2H_6, C_3H_6, C_3H_8, C_4H_8, and C_4H_{10} (Figure 6c) at much higher rates in solvent systems (Figure 6a), with catalytic TONs of 3.0, 2.7, and 4.5 obtained in reactions catalyzed by the M-, V-, and L-clusters, respectively (Figure 6e).[45] A similar increase in activity can be achieved in the reduction of CO_2 by the three clusters upon substituting Eu^{II}-DTPA (in an aqueous buffer system) by SmI_2 (in an organic solvent; only in this case, the reduction of CO_2 can barely be detected in reactions with Eu^{II}-DTPA (Figure 6b).[44,46] Additionally, even in the presence of SmI_2, the three clusters display narrower product profiles (CH_4, C_2H_4, C_2H_6, C_3H_6, and C_3H_8; Figure 6d) and lower catalytic TONs (1.4, 1.8, and 2.3, respectively) (Figure 6f) in the reduction of CO_2 than in the reduction of CO.[45] This finding reaffirms CO_2 as a much poorer substrate than CO for the nitrogenase-type cofactors.

In contrast to their protein-bound counterparts, the M- and V-clusters display comparable CO-reducing activities upon isolation, as well as a tendency toward the formation of CH_4 as the major hydrocarbon product (Figure 6c). The CO_2-reducing activities of the two clusters, on the other hand, remain comparable both in the protein-bound and in the isolated states; however, both clusters are considerably more active upon isolation and show significantly increased CH_4/CO ratios in their product profiles (Figure 6d). Together, these observations demonstrate that the protein environment has an impact on the reactivity of the cofactor species. Although the TONs of cofactor-based reactions are rather moderate under the current reaction conditions, the fact that nitrogenase cofactor species are capable of the catalytic turnover of CO and CO_2 firmly establishes these clusters as catalysts in their own right. As such, this finding provides the first proof-of-concept for the feasibility of developing cofactor-based biomimetic catalysts for conversion of CO and CO_2 into hydrocarbon products under ambient conditions.

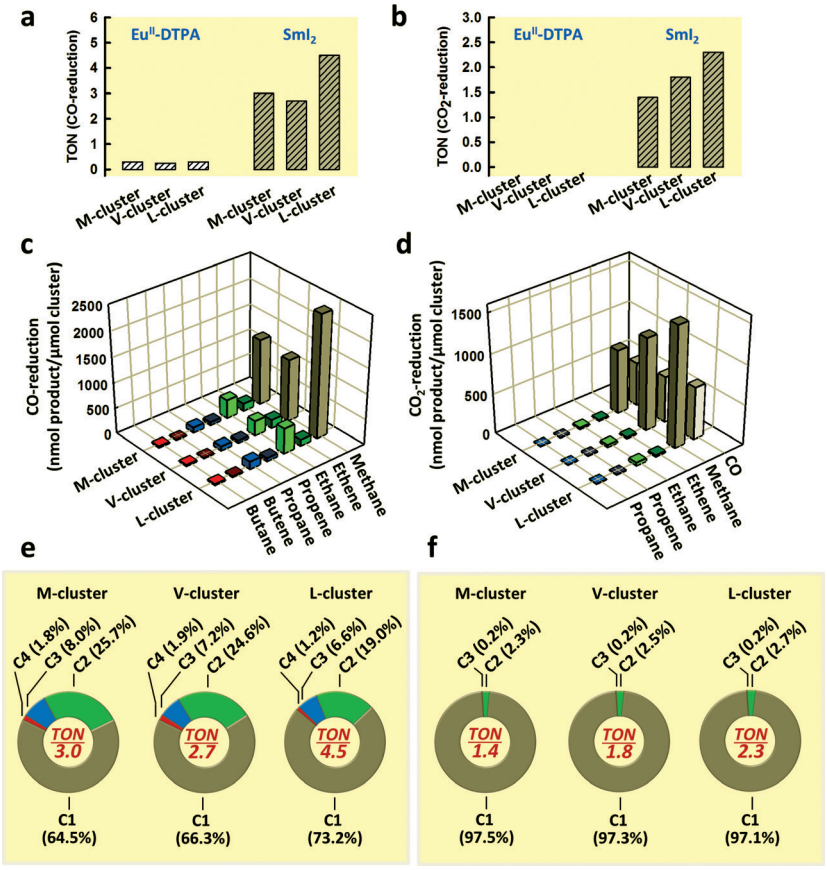

Figure 6. ATP-independent reduction of CO and CO_2 by nitrogenase cofactors. Shown are the TONs achieved with reductants Eu^{II}-DTPA and SmI_2 (a, b), yields of product formation with SmI_2 as the reductant (c, d), and product profiles with SmI_2 as the reductant (e, f) in the reactions of CO (a, c, e) and CO_2 (b, d, f) reduction by nitrogenase cofactors. The product profiles (e, f) show the percentages of C_1, C_2, C_3, and C_4 products. The TON was calculated from the nmol of carbon that appeared in the hydrocarbon products per nmol cofactor.

© 2016 Wiley-VCH Verlag GmbH & Co. KGaA, Weinheim

4. Central Carbide versus Carbon Coupling: Mechanistic Correlation between the Two?

The discovery of an interstitial carbide at the center of the nitrogenase cofactor[12,14] has raised mechanistically relevant questions of whether this carbide participates in the substrate turnover by nitrogenase and, if so, whether this carbide can be exchanged into the hydrocarbon products concomitant with the reductive C–C coupling by nitrogenase.[18] The identification of the SAM methyl group as the source of the interstitial carbide[19] provided a useful tool to address these questions, thus permitting the specific labeling of the central carbide with ^{14}C or ^{13}C isotopes and the subsequent tracing of the fate of the carbon isotope upon substrate turnover.[18]

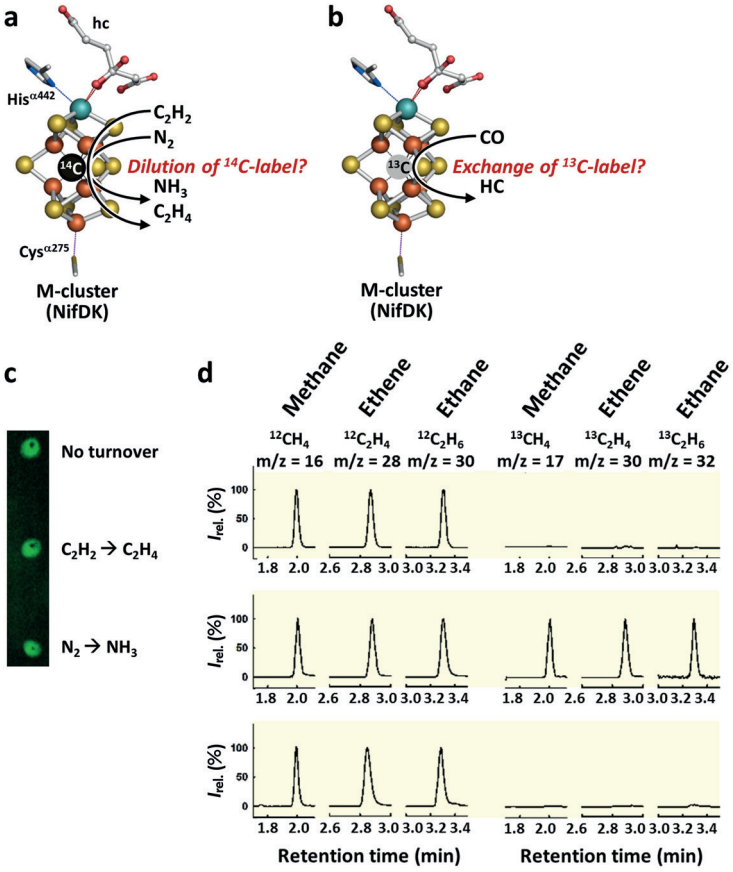

Figure 7. Tracing the interstitial carbide of the nitrogenase cofactor during substrate turnover. The interstitial carbide of the NifDK-bound M-cluster was labeled with a) ^{14}C to examine whether the ^{14}C label was diluted upon N_2 or C_2H_2 turnover; or b) ^{13}C to examine if the ^{13}C label was exchanged into the hydrocarbon (HC) products upon CO turnover. The M-cluster is depicted as described in Figure 1b. c) The intensities of the ^{14}C label in NifDK samples without turnover or upon turnover of C_2H_2 or N_2. Shown is the radiation of the ^{14}C label in the NifDK-bound M-cluster detected by autoradiography. The intensity of the ^{14}C label in the M-cluster did not change upon turnover of C_2H_2 or N_2, thus suggesting that the interstitial carbide remained in place in these reactions. d) GC-MS analysis of the hydrocarbon products generated from the turnover of ^{12}CO by unlabeled M-cluster (top traces), of ^{13}CO by unlabeled M-cluster (middle traces), and of ^{12}CO by ^{13}C-labeled M-cluster (bottom traces). No ^{13}C product was detected when ^{12}CO was turned over by the ^{13}C-labeled M-cluster (bottom right), which suggests that the interstitial carbide was not exchanged into products upon turnover.

4.1. The Fate of the Central Carbide upon Substrate Turnover

A combinatorial use of ^{14}C and ^{13}C isotopes was employed to trace the fate of the interstitial carbide of the M-cluster during turnover.[18] When [^{14}C]methyl-SAM was used to label the interstitial carbide of the M-cluster, the ^{14}C-labeled sample could be subjected to a fast turnover of substrates and subsequently examined for the amount of the ^{14}C label that remained in the M-cluster (Figure 7a). Conversely, when [^{13}C]methyl-SAM was used to label the interstitial carbide of the M-cluster, the ^{13}C-labeled sample could be subjected to a slow turnover of substrates and subsequently examined for the amount of the ^{13}C label that appeared in the products (Figure 7b). Interestingly, in the case of the ^{14}C-labeled sample, the intensity of the ^{14}C label in the cofactor sample remained unchanged after 3 h even upon rapid turnover of C_2H_2 and N_2 at a large molar excess to the interstitial carbide, which would have promoted a quick dilution of the ^{14}C label in the cofactor species (Figure 7c); whereas in the case of the ^{13}C-labeled sample, no ^{13}C-labeled product could be detected even with an extremely slow turnover of CO at a submolar ratio to the interstitial carbide, which would have prevented a quick dilution of the ^{13}C label in the hydrocarbon products (Figure 7d, lower traces). These results suggest that the interstitial carbide cannot be exchanged upon substrate turnover, nor can it be used as a substrate and incorporated into the products. A possible role can be proposed for the interstitial carbide based on these observations, one that is crucial for maintaining the structural integrity of the cofactor that underlies the functionality of nitrogenase during catalysis.

4.2. A Central Role of the Interstitial Carbide in C–C Coupling

Further support for the proposed role of the interstitial carbide in substrate turnover came from recent studies on CO binding to the cofactors of Mo- and V-nitrogenases.[52,54] Previously, spectroscopic analyses revealed the appearance of a unique EPR signal upon incubation of the Mo-nitrogenase with CO under turnover conditions, which was modeled as a single CO moiety bridged or semibridged between two Fe atoms across the "S-belt" of the M-cluster.[55–58] Consistent with this observation, a recent crystallographic study of the CO-bound M-cluster demonstrated that a CO moiety took the place of one belt-S atom and assumed a μ_2-coordination between two cross-belt Fe atoms (Figure 8a), a surprising observation that led to the proposal of a reactive iron species being generated upon displacement of the belt-S atom to accommodate the binding of CO.[54] Interestingly, a homologous conformation could be generated for the V-cluster by incubating the resting-state V-nitrogenase (i.e. the catalytic VnfDGK component alone) with CO in the presence of Eu^{II}-

 © 2016 Wiley-VCH Verlag GmbH & Co. KGaA, Weinheim

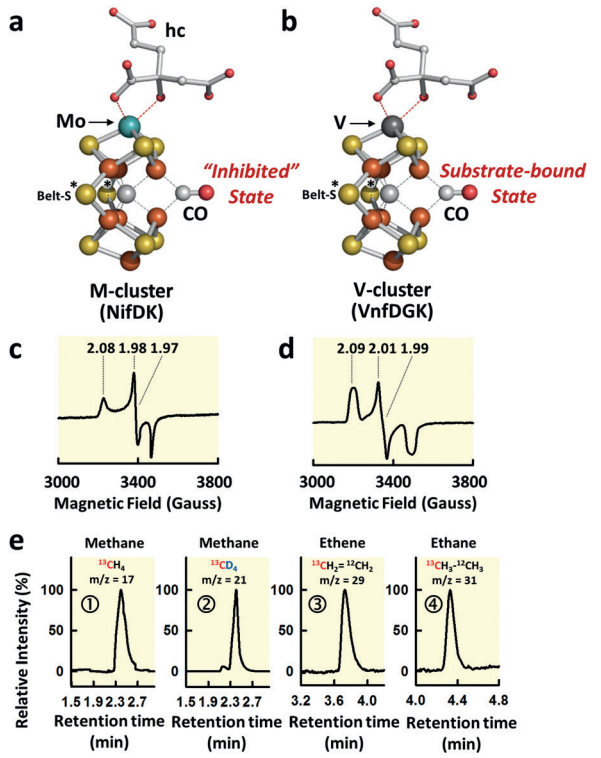

Figure 8. Homologous conformations of CO-bound M- and V-clusters. a) Crystal structure of the CO-bound M-cluster (an "inhibited" state) and b) homologous model of CO-bound V-cluster (a substrate-bound state). PDB entry 4TKV,[54] XAS/EXAFS,[51] and XES[52] data were used to generate these models. Atoms are colored as described in Figure 1b. The belt-S atoms are indicated by stars (*). Note that one of the three belt-S atoms is replaced by a CO moiety in the CO-bound conformations of both the M- and V-clusters. c,d) EPR features of c) the CO-bound M-cluster and d) the CO-bound V-cluster. The conformation of the CO-bound M-cluster was generated by incubating the turnover-state Mo-nitrogenase (i.e. NifH plus NifDK) with CO in the presence of dithionite and ATP, whereas the conformation of the CO-bound V-cluster was generated by incubating the resting-state V-nitrogenase (i.e. VnfDGK alone) with CO in the presence of the reductant Eu^{II}-DTPA ($E^{0'} = -1.14$ V at pH 8.0). Shown are difference spectra of samples prepared in the presence and absence of CO. The *g* values are indicated. e) The catalytic competence of the CO-bound V-cluster. GC-MS analysis of products formed upon turnover of the ^{13}CO-bound V-cluster in ① H_2O, and ② D_2O without extra CO (①,②) or in H_2O with 1% extra ^{12}CO (③, ④).

DTPA, which allowed the V-cluster to achieve a sufficiently low redox potential for CO binding without the extra push from turnover. The CO-bound M- and V-clusters displayed EPR signals with strikingly similar line shapes (Figure 8c,d),[52] thus suggesting a close resemblance between the two CO-bound conformations (Figure 8a,b).[52] However, while the "inhibited" state of the CO-bound M-cluster was hardly capable of turnover, the CO-bound V-cluster was catalytically competent and, thus, represented a substrate-bound state of nitrogenase. GC-MS analysis demonstrated that ^{13}CO could be preloaded onto the V-cluster and subsequently turned over into hydrocarbon products. In the absence of extra CO, turnover of the V-cluster-bound ^{13}CO resulted in the formation of $^{13}CH_4$ (Figure 8e, ①) and $^{13}CD_4$ (Figure 8e, ②) in H_2O and D_2O, respectively.[52] When 1% extra ^{12}CO was supplied, however, the V-cluster-bound ^{13}CO could also undergo reductive C–C coupling, thereby generating $^{13}CH_2{=}^{12}CH_2$ (Figure 8e, ③) and $^{13}CH_3$-$^{12}CH_3$ (Figure 8e, ④) as additional turnover products in H_2O-based reactions.[52]

The displacement of a belt-S atom by a CO moiety—a binding mode that is likely adopted by the catalytically competent conformation of the CO-bound V-cluster—points to a nitrogenase-based mechanism of CO activation that relies on a substantial rearrangement of the belt-S atom to uncover and activate the two Fe sites for the initial binding of CO and, possibly, the subsequent attachment of additional CO moieties for C–C coupling. The flexibility of the S-belt in this process suggests a critical role of the interstitial carbide in providing a strong anchor for the reactive Fe sites during ligand exchange, thereby maintaining the structural integrity of the cofactor while permitting significant restructuring of the S-belt that is crucial for substrate turnover. The function of the interstitial carbide, therefore, far exceeds that of a mere structural element. Although it may not directly participate in reduction of the substrate, this atom has a central role—both in location and function—in orchestrating the restructuring events of the cofactor that underlie the unique reactivity of nitrogenase toward CO.

5. Summary and Outlook

A close relationship between nitrogenase and carbon was unveiled through the identification of an interstitial carbide in the central cavity of the nitrogenase cofactor and the discovery of the ability of nitrogenase to catalyze the reductive C–C coupling of small carbon compounds. Subsequent investigations of the carbide insertion pathway revealed a novel, radical-SAM-dependent route to generate complex, bridged metalloclusters, whereas recent studies of CO activation implied a crucial, albeit indirect role of the interstitial carbide in upholding the structural integrity while facilitating substantial restructuring of the cofactor during substrate turnover.

However, many questions remain unanswered regarding the exact correlations of these carbon species to the assembly and catalytic mechanisms of nitrogenase. With regard to carbide insertion, details of events that further process the carbon intermediate into a carbide ion, as well as those related to the origin of the ninth sulfur and the radical-based cluster rearrangement, are yet to be explored to elucidate the assembly mechanism of the nitrogenase cofactor. In terms of C–C coupling, further examination of the activation mechanism of carbon species, as well as continued optimization of the reaction conditions for C–C coupling, is required to understand the reactivity of nitrogenase toward carbon compounds and develop strategies for future biotechnological adaptations of these reactions for converting carbon wastes into useful hydrocarbon products. Although there is a long way to go to achieve these goals, further investigations into the relationship between nitrogenase and carbon promise to advance our understanding of the mechanism of nitrogenase and unveil unprecedented chemical reactions catalyzed by this fascinating enzyme system.

 © 2016 Wiley-VCH Verlag GmbH & Co. KGaA, Weinheim

Acknowledgements

This work was supported by NIH grant GM-67626 (M.W.R.), DOE (BES) Award DE-SC0014470 (M.W.R. and Y.H.), and the Hellman foundation (Y.H.)

How to cite: *Angew. Chem. Int. Ed.* **2016**, *55*, 8216–8226
Angew. Chem. **2016**, *128*, 8356–8367

[1] B. K. Burgess, D. J. Lowe, *Chem. Rev.* **1996**, *96*, 2983–3012.
[2] J. B. Howard, D. C. Rees, *Chem. Rev.* **1996**, *96*, 2965–2982.
[3] B. M. Hoffman, D. Lukoyanov, Z. Y. Yang, D. R. Dean, L. C. Seefeldt, *Chem. Rev.* **2014**, *114*, 4041–4062.
[4] Although the ATP-dependent reduction of CO_2 by nitrogenase is subcatalytic, preliminary studies have demonstrated catalytic turnover of CO_2 by isolated nitrogenase cofactors when combined with a proper reductant in an organic solvent system.
[5] Y. Hu, C. C. Lee, M. W. Ribbe, *Dalton Trans.* **2012**, *41*, 1118–1127.
[6] Y. Hu, C. C. Lee, M. W. Ribbe, *Science* **2011**, *333*, 753–755.
[7] C. C. Lee, Y. Hu, M. W. Ribbe, *Science* **2010**, *329*, 642.
[8] Z. Y. Yang, D. R. Dean, L. C. Seefeldt, *J. Biol. Chem.* **2011**, *286*, 19417–19421.
[9] R. Schlögl, *Angew. Chem. Int. Ed.* **2003**, *42*, 2004–2008; *Angew. Chem.* **2003**, *115*, 2050–2055.
[10] C. K. Rofer-DePoorter, *Chem. Rev.* **1981**, *81*, 447–474.
[11] O. Einsle, F. A. Tezcan, S. L. Andrade, B. Schmid, M. Yoshida, J. B. Howard, D. C. Rees, *Science* **2002**, *297*, 1696–1700.
[12] T. Spatzal, M. Aksoyoglu, L. Zhang, S. L. Andrade, E. Schleicher, S. Weber, D. C. Rees, O. Einsle, *Science* **2011**, *334*, 940.
[13] J. Kim, D. C. Rees, *Nature* **1992**, *360*, 553–560.
[14] K. M. Lancaster, M. Roemelt, P. Ettenhuber, Y. Hu, M. W. Ribbe, F. Neese, B. Bergmann, S. DeBeer, *Science* **2011**, *334*, 974–977.
[15] F. A. Tezcan, J. T. Kaiser, D. Mustafi, M. Y. Walton, J. B. Howard, D. C. Rees, *Science* **2005**, *309*, 1377–1380.
[16] H. Schindelin, C. Kisker, J. L. Schlessman, J. B. Howard, D. C. Rees, *Nature* **1997**, *387*, 370–376.
[17] J. A. Wiig, Y. Hu, M. W. Ribbe, *Nat. Commun.* **2015**, *6*, 8034.
[18] J. A. Wiig, C. C. Lee, Y. Hu, M. W. Ribbe, *J. Am. Chem. Soc.* **2013**, *135*, 4982–4983.
[19] J. A. Wiig, Y. Hu, C. C. Lee, M. W. Ribbe, *Science* **2012**, *337*, 1672–1675.
[20] M. W. Ribbe, Y. Hu, K. O. Hodgson, B. Hedman, *Chem. Rev.* **2014**, *114*, 4063–4080.
[21] L. Zheng, R. H. White, V. L. Cash, D. R. Dean, *Biochemistry* **1994**, *33*, 4714–4720.
[22] L. Zheng, R. H. White, V. L. Cash, R. F. Jack, D. R. Dean, *Proc. Natl. Acad. Sci. USA* **1993**, *90*, 2754–2758.
[23] P. C. Dos Santos, D. C. Johnson, B. E. Ragle, M. C. Unciuleac, D. R. Dean, *J. Bacteriol.* **2007**, *189*, 2854–2862.
[24] A. D. Smith, G. N. L. Jameson, P. C. Dos Santos, J. N. Agar, S. Naik, C. Krebs, J. Frazzon, D. R. Dean, B. H. Huynh, M. K. Johnson, *Biochemistry* **2005**, *44*, 12955–12969.
[25] P. Yuvaniyama, J. N. Agar, V. L. Cash, M. K. Johnson, D. R. Dean, *Proc. Natl. Acad. Sci. USA* **2000**, *97*, 599–604.
[26] L. M. Zheng, D. R. Dean, *J. Biol. Chem.* **1994**, *269*, 18723–18726.
[27] J. A. Wiig, Y. Hu, M. W. Ribbe, *Proc. Natl. Acad. Sci. USA* **2011**, *108*, 8623–8627.
[28] J. T. Kaiser, Y. Hu, J. A. Wiig, D. C. Rees, M. W. Ribbe, *Science* **2011**, *331*, 91–94.
[29] A. W. Fay, M. A. Blank, C. C. Lee, Y. Hu, K. O. Hodgson, B. Hedman, M. W. Ribbe, *Angew. Chem. Int. Ed.* **2011**, *50*, 7787–7790; *Angew. Chem.* **2011**, *123*, 7933–7936.
[30] M. C. Corbett, Y. Hu, A. W. Fay, M. W. Ribbe, B. Hedman, K. O. Hodgson, *Proc. Natl. Acad. Sci. USA* **2006**, *103*, 1238–1243.
[31] K. M. Lancaster, Y. Hu, U. Bergmann, M. W. Ribbe, S. Debeer, *J. Am. Chem. Soc.* **2013**, *135*, 610–612.
[32] Y. Hu, A. W. Fay, M. W. Ribbe, *Proc. Natl. Acad. Sci. USA* **2005**, *102*, 3236–3241.
[33] Y. Hu, M. C. Corbett, A. W. Fay, J. A. Webber, K. O. Hodgson, B. Hedman, M. W. Ribbe, *Proc. Natl. Acad. Sci. USA* **2006**, *103*, 17125–17130.
[34] Y. Hu, M. C. Corbett, A. W. Fay, J. A. Webber, K. O. Hodgson, B. Hedman, M. W. Ribbe, *Proc. Natl. Acad. Sci. USA* **2006**, *103*, 17119–17124.
[35] J. M. Yoshizawa, B. A. Blank, A. W. Fay, C. C. Lee, J. A. Wiig, Y. Hu, K. O. Hodgson, B. Hedman, M. W. Ribbe, *J. Am. Chem. Soc.* **2009**, *131*, 9321–9325.
[36] Y. Hu, M. W. Ribbe, *J. Biol. Chem.* **2013**, *288*, 13173–13177.
[37] J. Christiansen, P. J. Goodwin, W. N. Lanzilotta, L. C. Seefeldt, D. R. Dean, *Biochemistry* **1998**, *37*, 12611–12623.
[38] B. Schmid, M. W. Ribbe, O. Einsle, M. Yoshida, L. M. Thomas, D. R. Dean, D. C. Rees, B. K. Burgess, *Science* **2002**, *296*, 352–356.
[39] A. W. Fay, J. A. Wiig, C. C. Lee, Y. Hu, *Proc. Natl. Acad. Sci. USA* **2015**, *112*, 14829–14833.
[40] G. R. Dukes, R. H. Holm, *J. Am. Chem. Soc.* **1975**, *97*, 528–533.
[41] R. C. Job, T. C. Bruice, *Proc. Natl. Acad. Sci. USA* **1975**, *72*, 2478–2482.
[42] J. G. Rebelein, Y. Hu, M. W. Ribbe, *ChemBioChem* **2015**, *16*, 1993–1996.
[43] J. G. Rebelein, Y. Hu, M. W. Ribbe, *Angew. Chem. Int. Ed.* **2014**, *53*, 11543–11546; *Angew. Chem.* **2014**, *126*, 11727–11730.
[44] C. C. Lee, Y. Hu, M. W. Ribbe, *mBio* **2015**, *6*, e00307-15.
[45] C. C. Lee, Y. Hu, M. W. Ribbe, *Angew. Chem. Int. Ed.* **2015**, *54*, 1219–1222; *Angew. Chem.* **2015**, *127*, 1235–1238.
[46] C. C. Lee, Y. Hu, M. W. Ribbe, *Angew. Chem. Int. Ed.* **2012**, *51*, 1947–1949; *Angew. Chem.* **2012**, *124*, 1983–1985.
[47] R. R. Eady, *Chem. Rev.* **1996**, *96*, 3013–3030.
[48] Y. Hu, M. W. Ribbe, *J. Biol. Inorg. Chem.* **2015**, *20*, 435–445.
[49] M. A. Blank, C. C. Lee, Y. Hu, K. O. Hodgson, B. Hedman, M. W. Ribbe, *Inorg. Chem.* **2011**, *50*, 7123–7128.
[50] Y. Hu, M. C. Corbett, A. W. Fay, J. A. Webber, B. Hedman, K. O. Hodgson, M. W. Ribbe, *Proc. Natl. Acad. Sci. USA* **2005**, *102*, 13825–13830.
[51] A. W. Fay, M. A. Blank, C. C. Lee, Y. Hu, K. O. Hodgson, B. Hedman, M. W. Ribbe, *J. Am. Chem. Soc.* **2010**, *132*, 12612–12618.
[52] C. C. Lee, A. W. Fay, T. C. Weng, C. M. Krest, B. Hedman, K. O. Hodgson, Y. Hu, M. W. Ribbe, *Proc. Natl. Acad. Sci. USA* **2015**, *112*, 13845–13849.
[53] V. K. Shah, W. J. Brill, *Proc. Natl. Acad. Sci. USA* **1977**, *74*, 3249–3253.
[54] T. Spatzal, K. A. Perez, O. Einsle, J. B. Howard, D. C. Rees, *Science* **2014**, *345*, 1620–1623.
[55] L. M. Cameron, B. J. Hales, *Biochemistry* **1998**, *37*, 9449–9456.
[56] Z. Maskos, B. J. Hales, *J. Inorg. Biochem.* **2003**, *93*, 11–17.
[57] H. I. Lee, L. M. Cameron, B. J. Hales, B. M. Hoffman, *J. Am. Chem. Soc.* **1997**, *119*, 10121–10126.
[58] H. I. Lee, M. Sørlie, J. Christiansen, T. C. Yang, J. Shao, D. R. Dean, B. J. Hales, B. M. Hoffman, *J. Am. Chem. Soc.* **2005**, *127*, 15880–15890.

Received: January 1, 2016
Published online: May 20, 2016

 © 2016 Wiley-VCH Verlag GmbH & Co. KGaA, Weinheim